ARTIFICIAL SATELLITES, Vol. 57, No. SI1 – 2022
DOI: 10.2478/arsa-2022-0023

EARTH ROTATION PARAMETERS PREDICTION AND CLIMATE CHANGE INDICATORS IN IT

Xueqing XU[1–3], Yonghong ZHOU[1–3], Cancan XU[1,3]

[1] Shanghai Astronomical Observatory, Chinese Academy of Sciences, Shanghai, China
[2] Key Laboratory of Planetary Sciences, Chinese Academy of Sciences, Shanghai, China
[3] School of Astronomy and Space Science, University of Chinese Academy of Sciences, Beijing, China

e-mails: xqxu@shao.ac.cn, yhzhou@shao.ac.cn, ccxu@shao.ac.cn

ABSTRACT. As one of the participants in the Second Earth Orientation Parameters Prediction Comparison Campaign (2nd EOP PCC), we submitted two data files. One is 365 days' predictions into the future for Earth orientation parameters (EOP) (the position parameters Px and Py, the time parameters UT1-UTC and length of day changes ΔLOD), processed by the traditional least-square and autoregressive (LS + AR) model. Another is 90 days' predictions by the combined least-square and convolution method (LS + Convolution), with effective angular momentum (EAM) from Earth System Modelling GeoForschungsZentrum in Potsdam (ESMGFZ). Results showed that the LS + Convolution method performed better than the LS + AR model in short-term EOP predictions within 10 days, while the traditional LS + AR model presented higher accuracy in medium-term predictions over 10–90 days. Furthermore, based on the climate change information in Earth's rotation (mainly in the interannual variations of LOD), the climate change indicators are investigated with ΔLOD observations and long-term predictions. After two intermediate La Nina events were detected in the climate-related ΔLOD observations during the period of 2020–2022, another stronger La Nina phenomenon is indicated in the climate-related ΔLOD long-term predictions.

Keywords: EOP prediction, effective angular momentum, interannual ΔLOD, climate change indicators

1. INTRODUCTION

Variations in Earth rotation can be expressed by the Earth orientation parameters, which is abbreviated as EOP (mainly containing the position variations Px and Py, the time parameters UT1-UTC and length of day changes ΔLOD). EOP interlink conversion between the terrestrial and celestial reference systems, have important applications in many areas such as deep space exploration, satellite precise orbit determination and astrogeodynamics. As the EOP obtained by the space geodetic technologies have several days to weeks delay, the growing demands for modern space campaigns make high-precision short-medium-term (1–90 days) EOP predictions a worthy topic and initiate many researches.

In recent decades, single or hybrid mathematical models have been employed to EOP predictions, such as the least-square extrapolation (LS) and autoregressive (AR) model (Wu et al. 2019; Xu et al. 2015), spectral analysis combined with LS (Zotov et al. 2018; Guo et al. 2013), artificial neural networks (ANN) (Lei et al. 2017; Schuh et al. 2002), wavelet decomposition and auto-covariance method (Su et al. 2014; Kosek et al. 2005) and Kalman filter (Xu et al. 2012; Gross et al. 1998). Considering the contributions of the surface fluid (atmospheric and oceanic angular momentum [AAM and OAM, respectively]), numerous studies have added these geophysical excitations to improve EOP predictions (Modiri et al. 2020; Dill et al. 2019; Wang et al. 2014).

Among these mathematical models, results of the EOP prediction comparison campaign (EOP PCC) which took place during 2005–2009 revealed that no particular prediction technique is superior to others for all EOP components and all prediction intervals, while the LS + AR method shows advantage on average (Kalarus et al. 2010). The second EOP PCC was launched in July 2021, aiming to compare and evaluate the latest status of various EOP forecasts conducted by different institutes all over the world. As one of the participants of this campaign, we have summited two data files processed by the traditional LS + AR model and the LS + Convolution method, respectively. In the LS + Convolution method, the geophysical excitations including the OAM and AAM from the Earth System Modelling GeoForschungsZentrum in Potsdam (ESMGFZ) effective angular momentum (EAM) data sets are introduced.

Keeping with the angular momentum conservation of the Earth's ocean–atmosphere system, the forced angular momentum variations will cause opposite perturbations in the solid Earth, resulting in Earth's rotation changes. Based on this correlation, numerous studies have been carried out on the contributions of EOP from different geophysical sources. The results show that surface fluid becomes the primary source of interannual, seasonal and sub-seasonal variations of the Earth's rotation (Haddad and Bonaduce 2017; Zhou et al. 2008).

As a strong ocean–atmosphere coupling process on interannual scales, the El Nino-Southern Oscillation (ENSO) is a significant component of global weather and climate change. In other words, ENSO and Earth's rotation changes are closely related (Zotov et al. 2022; Lambert et al. 2017; Dickey et al. 2007). Moreover, the climate-related ΔLOD discussed in the latest work is suggested as a climate change indicator (Xu et al. 2022). Thus, this study focuses on the relationship between ENSO and the interannual variations of the Earth's rotation rate. Based on the interannual variability characteristics of ENSO events, we try to extract the climate change information both from ΔLOD observations and long-term (1-year) predictions.

The structure of the paper is as follows: the model and method employed for EOP predictions are described in Section 2; the data processing and analyses are discussed in Section 3; results are assessed and discussed in Section 4 and a summary of the main findings is provided in Section 5.

2. MODEL AND METHOD

This study selects the LS + AR model and LS + Convolution method to obtain EOP predictions. The root mean square error (RMSE) is chosen as a quality measure.

2.1. The LS + AR model

As complex variations of the Earth's rotation, there are commonly relative regular and irregular signals coupling in EOP data series, such as the trend, annual, Chandler terms and high-frequency trembles in polar motion and the trend, interannual, seasonal and sub-seasonal oscillations in ΔLOD. For the predictions of these stable signals, we adopt the LS model

expressed by polynomial trend and harmonic oscillations, and a stochastic process AR model can be employed for the predictions of irregular variations (Xu et al. 2015, 2012).

The LS model could be presented as

$$\begin{aligned} m_{regular}(t) &= a + bt + c_c \cos\left(\frac{2\pi t}{T_1}\right) + c_s \sin\left(\frac{2\pi t}{T_1}\right) \\ &+ d_c \cos\left(\frac{2\pi t}{T_2}\right) + d_s \sin\left(\frac{2\pi t}{T_2}\right) + ... \end{aligned} \tag{1}$$

where

$m(t)$ is the EOP data time series,

$a, b, c_c, c_s, d_c, d_s, ...$ are the LS model fitting parameters and

$T_1, T_2, ...$ are the periods of regular terms in EOP series. In the case of polar motion, the predominant oscillations are annual and Chandler $T_1 = 365.24\ d,\ T_2 = 433\ d$; for ΔLOD, the prominent periodic terms are annual and semi-annual $T_1 = 365.24\ d,\ T_2 = 182.6\ d$.

The rest of the LS fitting terms are then processed by the AR model; for a stationary random sequence $m_{iregular}$, the AR model is expressed as

$$m_{regular}(t) = \sum_{i=1}^{P} \varphi_i m(t-i) + a_i \tag{2}$$

where

a is the zero-mean white noise,

P is the order of AR model, which could be determined by the final prediction error (FPE) criterion and corresponds to the smallest FPE (Akaike 1971) and

φ is the autoregressive coefficient of the AR model, which could be obtained by solving the Yule-Walker equations with Levinson–Durbin recursion (Brockwell and Davis 1996).

2.2. The LS + Convolution method

In the LS + Convolution method, the EAM from ESMGFZ is selected as the input excitation series (using only the main contributions AAM and OAM). Firstly, the EAM series are predicted by the commonly used LS + AR model. Secondly, the interannual, seasonal and sub-seasonal terms of EOP are calculated from the EAM predictions by Liouville convolution equation. Meanwhile, the rest of EOP trend terms are extrapolated by the polynomial LS model. Finally, the total EOP predictions are combined by the excitation calculations and trend extensions (throughout the paper, this is abbreviated as the LS + Convolution method).

Liouville convolution equation describes the relationship between theoretical EOP $m(t)$ and excitation function $\psi(t)$ (Eubanks 1993; Gross 1992) as follows:

$$\begin{cases} \boldsymbol{m}(t) = m(0)e^{i\sigma_c t} - i\sigma_c \int_0^t \psi(t')e^{i\sigma_c(t-t')}dt' \\ \boldsymbol{m}_3(t) = \psi_3 + constant \end{cases} \tag{3}$$

where

A, C are the principal moments of inertia,
Ω is the average angular velocity of the Earth and
$\sigma_c = \frac{C-A}{A}\Omega$ is the Chandler frequency.

Considering the viscoelasticity of the Earth, the real number σ_c should be replaced by the complex one $\boldsymbol{\sigma}_c = \frac{2\pi}{T_c}\left(1 + \frac{i}{2Q_c}\right)$. Here, $T_c = 433d$ and $Q_c = 60$ represent the period and attenuation factor of Chandler wobble, respectively (Seitz et al. 2005).

The excitation function $\psi(t)$ in Equation 3 can be expressed as

$$\begin{cases} \psi_1 = \frac{1}{\Omega^2(C-A)}\left(\Omega^2 \Delta I_{13} + \Omega h_1 + \Omega \Delta \dot{I}_{23} + \dot{h}_2 - \Gamma_2\right) \\ \psi_2 = \frac{1}{\Omega^2(C-A)}\left(\Omega^2 \Delta I_{23} + \Omega h_2 - \Omega \Delta \dot{I}_{13} - \dot{h}_1 - \Gamma_1\right) \\ \psi_3 = \frac{1}{\Omega^2 C}\left(-\Omega^2 \Delta I_{33} - \Omega h_3 + \Omega \int_0^t \Gamma_3 dt'\right) \end{cases} \tag{4}$$

where

$\psi(t)$ is the excitation source induced by surface fluid and luni-solar torques,
$\Delta I(t)$ is the perturbation term of the Earth's inertia tensor, also called the mass term,
$\boldsymbol{h}(t)$ is the relative angular momentum and is also named as the motion term.

Regarding that there are no high-frequency terms (with period shorter than 2 days) in the conventional EOP observations, the theoretical EOP $\boldsymbol{m}(t)$ is equal to the observed EOP without more translations (Gross 1992).

2.3. The prediction precision indicator

Among many indicators of the prediction precision, the RMSE is a quality measure and is represented in Equation 5.

$$RMSE_j = \sqrt{\frac{1}{n}\sum_{i=1}^{n}(P_i^j - O_i^j)^2} \tag{5}$$

where

O are the EOP observations,
P are the EOP predictions,
j is the prediction span (interval in the future) and
n is the number of predictions used to calculate statistics.

3. DATA PROCESSING AND ANALYSES

Taking advantage of modern space technologies, the EOP observations have been greatly improved since 1980. So, this study focuses on the period from January 1980 to April 2022. Both the EOP and EAM data have been selected with all available epochs up to 1 day before the first prediction. The input EOP series contain combined and rapid solutions coming from the International Earth Rotation and Reference Systems Service (IERS) (Ratcliff and Gross 2019; Gambis 2004) (https://www.iers.org/IERS/EN/DataProducts/EarthOrientationData/eop.html). In data processing, the tidal terms in EOP are corrected by the IERS 2010 zonal tidal model (Gerard

and Brian 2010). In convolution calculations, the EAM series are obtained from ESMGFZ (Dobslaw and Dill, 2018) (http://esmdata.gfz-potsdam.de:8080/). In climate change analysis, the ENSO indices are obtained from the National Oceanic and Atmospheric Administration (NOAA) (https://origin.cpc.ncep.noaa.gov/products/analysis_monitoring/ensostuff/ONI_v5.php).

3.1. The excitation function series

Based on the correlations between EOP observations and geophysical excitation sources expressed by Liouville equation, we can calculate the EOP from excitation function directly. The excitation function series utilized in this study is the EAM from ESMGFZ, mainly arising from atmospheric and oceanic angular momentum changes. The time span of EAM series is from 1976 till now with a sampling interval of 3 h and is then averaged to 1 day to be consistent with that of EOP series. To illustrate the prominent contributions from surface fluid forcing, the interannual, seasonal and sub-seasonal variations extracted from IERS C04 EOP observations are compared in Figure 1 with the convoluted EOP from EAM series.

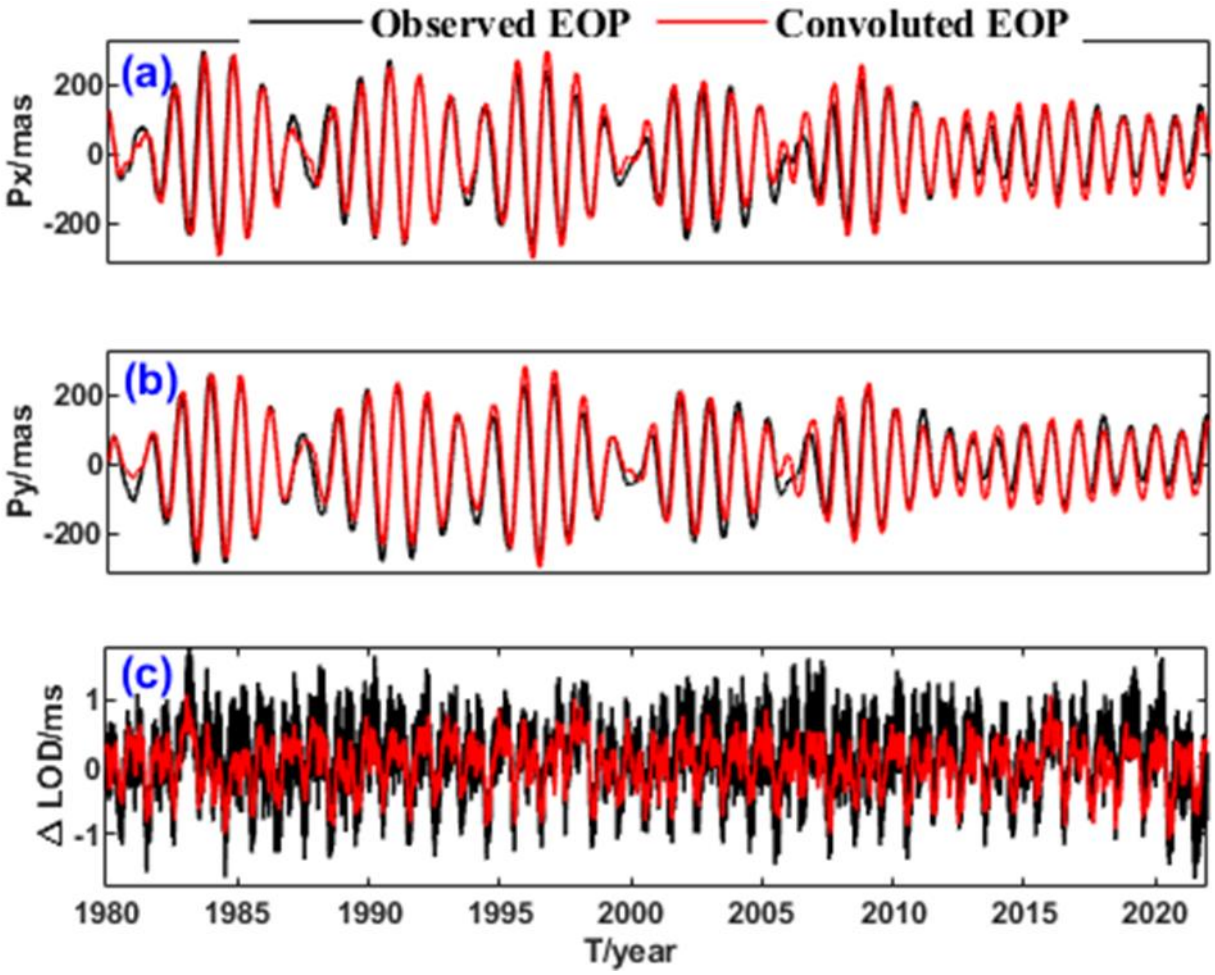

Figure 1. EOP interannual, seasonal and sub-seasonal terms extracted from IERS C04 observations (black line) and convoluted from the EAM series (red line) during 1980-2022.
(a) Px, (b) Py and (c) ΔLOD

As apparent from Figure 1a and b, after removing the trend terms, the polar motion sequences mainly contain the annual and Chandler oscillations and can be explained well by the EAM convolutions. Compared to polar motion, the EAM contributions to ΔLOD in Figure 1c are not that prominent. After removing the tidal and trend terms, ΔLOD series can be accounted for by

EAM contributions mostly. The remaining discrepancy may be ascribed to EAM model errors and other sources associated with interior processes (Hsu et al. 2021; Dobslaw and Dill, 2018). In addition, the same conclusions have been confirmed with other angular momentum data sets given by the National Center for Environmental Prediction/National Center for Atmospheric Research (NCEP/NCAR) reanalysis project and Estimating the circulation and Climate of the Ocean (ECCO) model (Chen et al. 2019; Bizouard et al. 2011).

3.2. The climate-related variations in LOD series

As climate change indicators in Earth's rotation, LOD variations on interannual scales have been discussed extensively. Besides, the latest study reveals that there are three signals (at ~6, ~7 and ~8 years) in ΔLOD interpreted as internal causes (Hsu et al. 2021), and these fluctuations need to be removed to obtain the interannual ΔLOD solely related to climatic variations. Considering all these effects from the trend terms, tidal variations and fluctuations due to internal causes, the time series of climate-related ΔLOD are displayed in Figure 2 after a rigorous data processing flowchart (see Xu et al. 2022 for more details). To show consistency between the climate-related ΔLOD and ENSO indices, the Nino 3.4 of Oceanic Niño Index (ONI) from NOAA during the same time span is also presented in Figure 2.

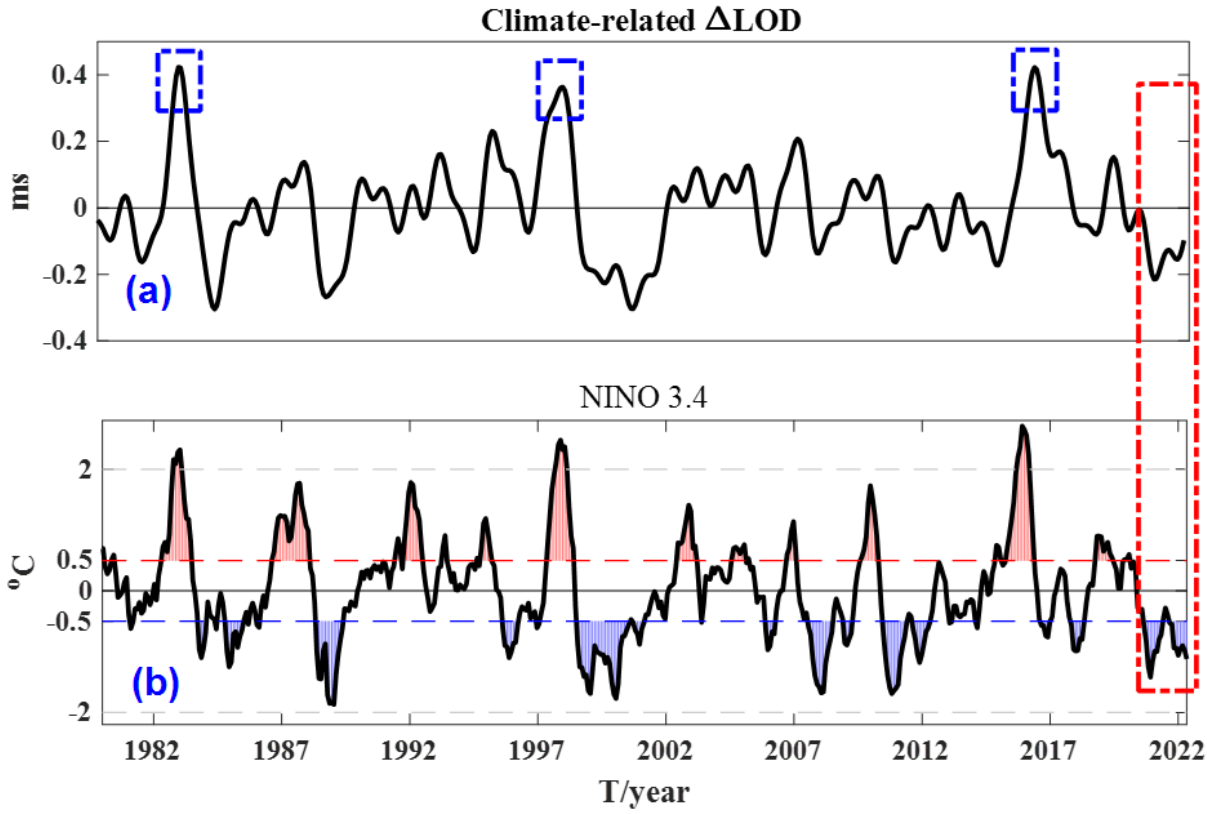

Figure 2. Monthly mean series of the climate-related ΔLOD and Nino 3.4 from January 1980 to April 2022. The blue square frames mark the three extreme El Nino events; the red square frame marks the latest two La Nina events during 2020–2022. (a) Climate-related ΔLOD and (b) Nino 3.4

Figure 2 shows that the climate-related ΔLOD and the ENSO indices exhibit similar positive and negative fluctuations, illustrating the speed decelerations and accelerations in Earth's rotation and corresponding to the El Nino (warm) and La Nina (cold) events in climate change, respectively. According to the NOAA determination conditions (sea surface temperature anomaly [SSTA] ≥0.5℃ or SSTA ≤–0.5℃ for more than 5 months), there were 11 El Nino and 14 La Nina events over decades and three extreme El Nino events occurred during 1982–

1983, 1997–1998 and 2015–2016 (Lambert et al. 2017). These events are identified in the observational record every time the equatorial Pacific SSTA is greater than 2.0°C for more than 5 months. To be specific, the clearly descending areas in interannual ΔLOD and ENSO indices are enclosed with a red square frame, pointing to the latest two La Nina events during 2020–2022. The minimum SSTA of approximately −1.3℃ and −1.0℃ occurred in November 2020 and December 2021, which could be both identified as intermediate strength. Furthermore, these two La Nina events forced the interannual ΔLOD to minimum values of approximately –0.22 and –0.19 ms, separately.

4. RESULTS

It is worth to note that the two parameters UT1-UTC and ΔLOD can be interconverted to each other. UT1-UTC is more commonly used in modern space applications, and ΔLOD is widely employed in scientific analysis. Thus, we just present accuracy results of the three predictions of Px, Py and UT1-UTC, but discuss climate change information in ΔLOD series.

4.1. EOP predictions

To evaluate EOP predictions carried out by the LS + AR and LS + Convolution methods, we estimate accuracy of 1–90 days' results over the second EOP PCC period of 07.2021–03.2022. These predictions were produced weekly, and the RMSE values of different forecasting spans are listed in Table 1. In order to illustrate the results more intuitively, the 1–90 days' RMSE values calculated from the two models are graphically shown in Figure 3. The red and dot line represents the RMSE for the LS + Convolution predictions, and the blue and dot line for the LS + AR predictions.

Table 1. RMSE of different EOP forecast spans obtained by the LS + AR and LS + CV methods over 07.2021–03.2022

Forecast span (days)	Px (mas)		Py (mas)		UT1-UTC (ms)	
	LS + AR	LS + CV	LS + AR	LS + CV	LS + AR	LS + CV
1	0.70	0.058	0.87	0.84	0.20	0.18
2	1.14	1.05	1.05	1.00	0.35	0.32
3	1.61	1.54	1.32	1.27	0.50	0.47
4	2.12	2.11	1.50	1.45	0.64	0.60
5	2.54	2.54	1.67	1.64	0.76	0.71
6	2.84	2.83	1.83	1.81	0.86	0.82
7	3.02	3.02	1.88	1.86	0.91	0.89
8	3.22	3.22	1.93	1.92	0.97	0.95
9	3.44	3.43	2.01	2.01	1.03	1.01
10	3.75	3.74	2.14	2.13	1.10	1.07
20	4.87	5.15	3.01	3.06	2.83	2.90
30	5.44	5.80	3.98	4.10	4.18	4.40
40	5.35	5.85	5.23	5.53	5.98	6.46
50	4.47	5.51	6.47	7.08	8.03	8.72

Forecast span (days)	Px (mas)		Py (mas)		UT1-UTC (ms)	
	LS + AR	LS + CV	LS + AR	LS + CV	LS + AR	LS + CV
60	4.32	4.82	7.33	8.12	9.98	10.85
70	5.27	5.44	8.17	9.08	11.63	12.47
80	6.00	6.22	9.09	10.04	13.20	14.18
90	6.10	6.13	9.52	10.32	15.13	16.04

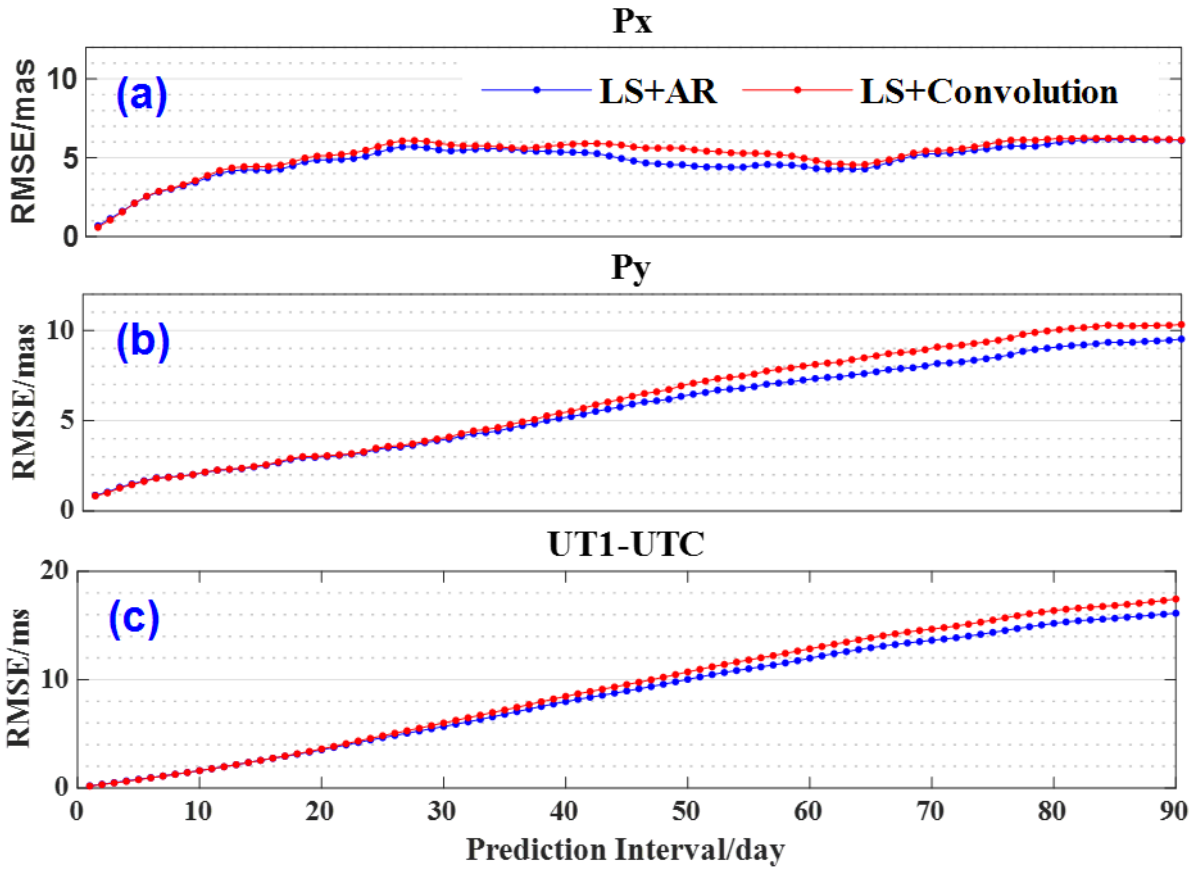

Figure 3. The 1–90 days' RMSE calculated from the LS + AR (blue dot line) and LS + Convolution (red dot line) model. (a) Px, (b) Py and (c) UT1-UTC

From the closely related prediction RMSE results in Table 1 and Figure 3, a preliminary finding could be summarized: in short-term EOP predictions within 10 days, the LS + Convolution (red dot line) method performs slightly better, while the traditional LS + AR model (blue dot line) shows significant improvements in medium-term predictions over 10–90 days.

4.2. Climate change information extracted from ΔLOD observations and predictions during 2020–2023

Regarding the consistent climate change information shown in interannual ΔLOD and ENSO indices in Section 3.2, here we try to investigate the climate change forecasts with ΔLOD long-term predictions, focusing on the period 2020–2023. Based on the accuracy estimates listed in Table 1, the LS + AR model is selected to obtain the long-term ΔLOD predictions. To make the prediction of the ENSO events more convincing, we have tried two forecasting tests of the latest two La Nina during 2020–2021 and 2021–2022 from ΔLOD predictions of 1 year over

the event. The climate-related variations extracted from different ΔLOD observations and predictions are compared in Figure 4.

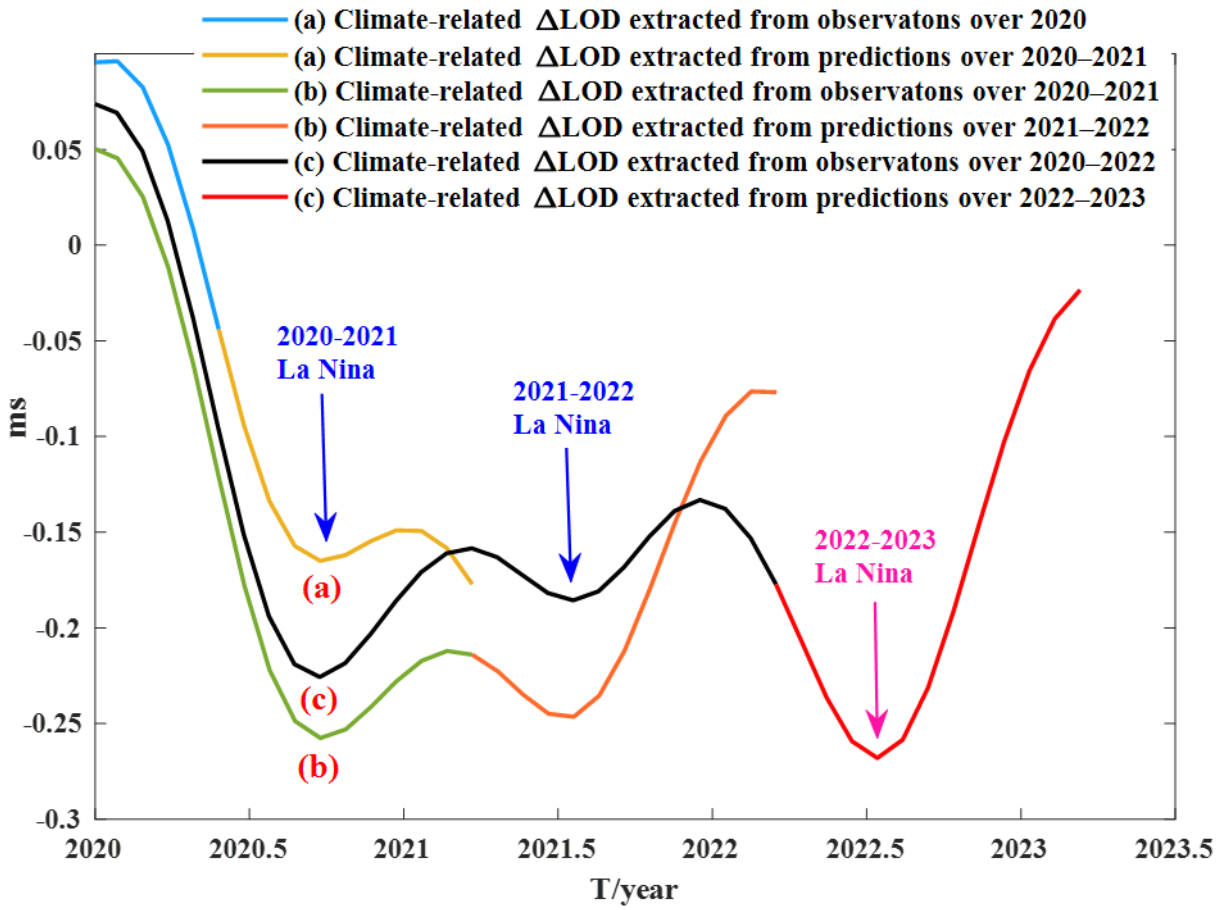

Figure 4. Climate change information extracted from ΔLOD observations and predictions: (a) 2020–2021 time span, (b) 2020–2022 time span and (c) 2020–2023 time span

Figure 4 illustrates the climate-related variations extracted from ΔLOD observations (blue, green and black curves) and predictions of 1 year into the future (yellow, orange and red curves). As can be seen in black curve (c), the latest two La Nina events during the periods 2020–2021 and 2021–2022 are marked with blue, with minimum values of approximately –0.22 and –0.19 ms, respectively. Compared to the variations extracted only from ΔLOD observations, the first forecasting test indicates the latest 2020–2021 La Nina event with a weaker strength (yellow curve (a), –0.16 ms), while the second test predicts the latest 2021–2022 La Nina with a bigger amplitude (orange curve (b), –0.25 ms). In summary, these two tests prove that the climate-related variations extracted from ΔLOD predictions could be indicators of climate change. After forecasting tests of the latest two ENSO events, the climate-related terms extracted from ΔLOD predictions of 1 year over 2022–2023 are denoted in the red cure (c). It can be seen that another stronger follow-up La Nina is predicted in the next year (marked with pink, –0.27 ms). Considering that the latest 2021–2022 La Nina is still in the process of development, this predicted minimum point may be a second trough continuing from the 2021–2022 phenomenon. The latest two La Nina events were suggested to be potential indicators of the Earth's rotation acceleration and series of extreme weather events (e.g. cold waves and strong rainfalls) in the recent two years; therefore, the next predicted trough needs more investigations and attention.

5. CONCLUSIONS

Angular momentum exchanges of the solid Earth with geophysical fluids as well as other forces excite the Earth's rotation changes, and their relationship can be depicted by Liouville equation, meaning that EOP and geophysical excitations could be interconverted to each other. This work reconstructs the interannual, seasonal and sub-seasonal EOP by Liouville equation, with geophysical excitations (AAM, OAM) from ESMGFZ during 1980–2022. Results show that the convoluted sequences match the observed EOP series well, which confirms the fluid contributions to EOP reported in previous studies.

Using the latest EAM series from ESMGFZ, we employed the LS + Convolution method to obtain 1–90 days' EOP predictions. As a comparison, the LS + AR method was also carried out. The RMSE statistics revealed that the LS + Convolution method performs better in short-term EOP predictions and the LS + AR model shows higher accuracy in medium-term predictions. We will introduce other small contributors (e.g. hydrological angular momentum) to EOP predictions in further convolution calculations.

In addition, two intermediate La Nina events during 2020–2022 were detected in both the climate-related ΔLOD and ENSO indices. Besides, the latest two La Nina events have been forecasted successfully with the verification experiments. Furthermore, another stronger La Nina phenomenon is predicted in the near future. Considering a series of severe weather events over the past 2 years, the whole society needs to pay close attention. We will continue to focus on this event in subsequent studies.

Acknowledgements. The research is supported by the B-type Strategic Priority Programme of the Chinese Academy of Sciences Grant (XDB41000000), the NSFC Grant (12173070, 11973010) and the Youth Innovation Promotion Association of Chinese Academy of Sciences (2019265). We thank the International Earth Rotation and Reference Systems Service (IERS) for providing the Earth orientation parameters' observations, the Effective Angular Momentum Functions from Earth System Modelling at GeoForschungsZentrum in Potsdam (ESMGFZ) for the EAM series and the National Oceanic and Atmospheric Administration (NOAA) for the Oceanic Niño Index (Nino 3.4).

REFERENCES

Akaike H. (1971). Autoregressive model fitting for control, *Ann Inst Stat Math*, 23, 163-180. Bizouard C., Remus F., Lambert S., Seoane L., Gambis D. (2011). The Earth's variable Chandler wobble, *A&A*, 526, A106.

Brockwell P.J., Davis R.A. (1996). Introduction to time series and forecasting, *Springer, New York*, 420.

Chen J.L., Wilson C.R., Kuang W.J., Chao B.F. (2019). Interannual oscillations in Earth rotation, *Journal of Geophysical Research: Solid Earth*, 124.

Dickey J.O., Marcus S.L., Chin T.M. (2007). Thermal wind forcing and atmospheric angular momentum: Origin of the Earth's delayed response to ENSO, *Geophysical Research Letters*, 34, 17803(1-5).

Dill R., Dobslaw H., Thomas M. (2019). Improved 90-day earth orientation predictions from angular momentum forecasts of atmosphere, ocean, and terrestrial hydrosphere, *Journal of Geodesy*, 93(3), 287-295.

Dobslaw H., Dill R. (2018). Predicting Earth Orientation Changes from Global Forecasts of Atmosphere-Hydrosphere Dynamics, *Adv. Space Res*, 61(4), 1047-1054.

Eubanks T.M., Smith D.E., Turcotte D.L. (1993). Variations in the orientation of the Earth, *Geodynamics Series*, 24, 1-54.

Gambis D. (2004). Monitoring Earth Orientation using space-geodetic techniques: state-of-the-art and prospective, *Journal of Geodesy*, 78, 295-303.

Guo J.Y., Li Y.B., Dai C.L., Shum C.K. (2013). A technique to improve the accuracy of Earth orientation prediction algorithms based on least squares extrapolation, *J. Geodyn* .70, 36-48.

Gerard P., Brian L. (2010). *IERS Conventions (2010)*, 50-126.

Gross R.S., Eubanks T.M., Steppe J.A., Freedman A.P., Dickey J.O., Runge T.F. (1998). A Kalman filter-based approach to combining independent Earth-orientation series, *J Geod*,72, 215-235.

Gross R.S. (1992). Correspondence between theory and observations of polar motion, *Geophys. J. In*, 109, 162-170.

Haddad M., Bonaduce A. (2017). Interannual variations in length of day with respect to El Niño- Southern Oscillation's impact (1962-2015), *Arab J Geosci*, 10(11), 1-10.

Hsu C.C., Duan P.S., Xu X.Q., Zhou Y.H., Huang C.L. (2021). A new ~7 year periodic signal in length of day from a FDSR method, *Journal of Geodesy*, 95:55.

Kalarus M., Schuh H., Kosek W., Akyilmaz O., Bizouard Ch., Gambis D., Gross R.S., Jovanovic B., Kumakshev S., Kutterer H., Mendes Cerveira P.J., Pasynok S., Zotov L. (2010). Achievements of the Earth orientation parameters prediction comparison campaign, *J Geod*, 84, 587-596.

Kosek W., Kalarus M., Johnson T. J., Wooden W.H., McCarthy D.D., Popinski W. (2005). A comparison of LOD and UT1–UTC forecasts by different combination prediction techniques, *Artificial Satellites*, 40, 119-125.

Lambert S.B., Marcus S.L., Viron O.D. (2017). Atmospheric torques and Earth's rotation: what drove the millisecond-level length-of-day response to the 2015-2016 El Nino? *Earth System Dynamics Discussions*, 8, 1-14.

Lei Y., Guo M., Hu D., Cai H., Zhao D., Hu Z., Gao Y. (2017). Short-term prediction of UT1-UTC by combination of the grey model and neural networks, *Adv Space Res*, 59(2), 524-531.

Modiri S., Belda S., Hoseini M., Heinkelmann R., Ferrándiz J., Schuh H. (2020). A new hybrid method to improve the ultra-short-term prediction of LOD, *J Geod*, 94, 23.

Ratcliff J., Gross R. (2019). Combinations of Earth Orientation Measurements: SPACE2018, COMB2018, and POLE2018, Pasadena, *CA: Jet Propulsion Laboratory, National Aeronautics and Space Administration*.

Seitz, F., & Schmidt, M. 2005. Atmospheric and oceanic contributions to Chandler Wobble excitation determined by wavelet filtering. *J. Geophy. Res*, 110, B11406.

Su X., Liu L., Hsu H., Wang G. (2014). Long-term polar motion prediction using normal time–frequency transform, *J Geod*, 88,145-155.

Schuh H., Ulrich M., Egger D., Muller J. (2002). Prediction of Earth orientation parameters by artificial neural networks, *J Geod*, 76, 247-258.

Wang Q., Du Y., Liu J. (2014). Introducing atmospheric angular momentum into prediction of length of day change by generalized regression neural network model, *J. Cent. South Univ*, 21, 1396-1401.

Wu F., Chang G., Deng K. (2019). One-step method for predicting LOD parameters based on LS+AR model, *J Spat Sci*.

Xu X.Q., Zhou Y.H., Duan P.S., Fang M., Kong Z.Y., Xu C.C., An X.R. (2022). Contributions of oceanic and continental AAM to interannual variation in ΔLOD with the detection of 2020–2021 La Nina event, *J Geod*, 96, 43.

Xu X.Q., Zhou Y.H. (2015). EOP prediction using least square fit in and autoregressive filter over optimized data intervals, *Adv. Space Res*, 56, 2248-2253.

Xu X.Q., Zhou Y.H., Liao X.H. (2012). Short-term earth orientation parameters predictions by combination of the least squares, AR model and Kalman filter, *J. Geodyn*, 62, 83-86.

Zhou Y.H., Chen J.L., Salstein D. (2008). Troposphere and stratospheric wind contributions to Earth's variable rotation from NCEP/NCAR reanalyses (2000-2005), *Geophysical Journal International*, 174, 453-463.

Zotov L., Bizouard C., Shum C.K., Zhang C.Y., Sidorenkov N., Yushkin V. (2022). Analysis of Earth's polar motion and length of day trends in comparison with estimates using second degree stokes coefficients from satellite gravimetry, *Advances in Space Research*, 69,308-318.

Zotov L., Xu X.Q., Zhou Y.H., Skorobogatov A. (2018). Combined SAI-SHAO prediction of Earth Orientation Parameters since 2012 till 2017, *Geodesy and Geodynamics*, 9(6), 485-490.

Received: *2022-06-28*

Reviewed: *2022-07-15 (undisclosed name); 2022-07-20 (L. Zotov)*

Accepted: *2022-08-16*